Broadband Infrared Imaging for Enhanced Gas Leak Detection

Jianzhi Fan[1], Jing Zhou[1,2], Qi Zhao[3], Dong Luo[1] and Wei Chen[1]
[1]*Shenzhen Institute of Advanced Technology, Chinese Academy of Sciences, 1068 Xueyuan Avenue, Shenzhen 518055, China*
[2]*School of Software Engineering, University of Science and Technology of China, 188 RenAi Road, Suzhou 215123, China*
[3]*School of Mechatronical Engineering, Beijing Institute of Technology, 5th South Zhongguancun Street, Beijing 100081, China*
{*jz.fan, dong.luo, chenwei*}*@siat.ac.cn, zhou_jing@mail.ustc.edu.cn, 3120245168@bit.edu.cn*

Keywords: Optical Gas Imaging, Passive Infrared Detection, Gas Leak Detection.

Abstract: This paper presents a passive broadband infrared imaging system designed for gas leak detection. The system utilizes an optical design optimized for the 3–14 μm range, including a wide-spectrum lens and an uncooled infrared camera. The broadband capability enables the detection of various gases across a wide spectral range. To identify gas leaks, a novel adaptive gas leakage detection algorithm based on YOLOX and traditional image processing techniques is developed. The system's performance is validated through field experiments with SF_6 and CO_2 gases, showcasing its ability to accurately detect and segment gas leakage regions. Furthermore, the study investigates the potential for gas composition analysis using the system's broadband imaging. Future work aims at optimizing the optical design and enhancing detection sensitivity for improved efficiency.

1 INTRODUCTION

Gas leaks in routine applications, industrial production, and transportation pose significant risks to public safety. Therefore, conducting rapid, sensitive, and accurate research on gas leak detection is of critical importance. From a practical perspective, the detection must locate the source within a large area rapidly and precisely. It should also measure the size, shape, and subsequent diffusion patterns of the gas cloud. This capability enables inspection personnel to promptly evaluate the severity of the leakage.

Traditional gas leak detection methods, such as gas chromatography (Moshayedi et al., 2023), electrochemical gas sensing (Tan et al., 2022), and photoacoustic spectroscopy (Zhao et al., 2022), employ point-measurement techniques. Despite their high sensitivity, these methods have a limited detection range that suited only for small-scale, close-range applications, and are inadequate for larger area assessments (Strahl et al., 2021). Furthermore, even when gas leaks are identified, due to the dispersion of leaked gas and varying wind speeds, it is difficult for personnel to accurately locate the source and comprehend current gas diffusion trends.

Many industrial gases have distinct absorption spectra in the mid- to long-wave infrared. Consequently, gas infrared imaging technology, which operates based on the principle of gas infrared absorption, enables real-time imaging of scenes and identification of leaked gases within the imagery. This innovative imaging approach can efficiently pinpoints leak sources and visualizes gas diffusion clouds, and is therefore increasingly applied in the field of gas detection (Wurst et al., 2017).

Infrared imaging technology for gas leak detection can be classified into active and passive types, depending on whether a laser or another active radiation source is utilized (Kulp et al., 1997). In certain scenarios, the use of a laser radiation source may enhance the signal-to-noise ratio (SNR) and thereby improve the system performance (Strahl et al., 2021). However, due to the varied infrared absorption characteristics of different gases and the restricted spectral range of radiation sources, the types of detectable gases are limited (Nutt et al., 2020). Additionally, as the operational distance increases, the intensity of the active radiation source diminishes rapidly, complicating long-range detection efforts. In contrast, passive infrared imaging technology does not require an active radiation source. It covers a broad spectral range, is capable of detecting a wide variety of gases, and facilitates long-distance imaging.

Recent advancements in uncooled infrared focal plane array (IRFPA) detectors have significantly enhanced the feasibility of thermal imaging for gas leak

Fan, J., Zhou, J., Zhao, Q., Luo, D. and Chen, W.
Broadband Infrared Imaging for Enhanced Gas Leak Detection.
DOI: 10.5220/0013152300003902

In *Proceedings of the 13th International Conference on Photonics, Optics and Laser Technology (PHOTOPTICS 2025)*, pages 102-108
ISBN: 978-989-758-736-8; ISSN: 2184-4364

detection. Regular infrared cameras, however, are typically limited in either the mid-infrared (3–5 μm) or the long-infrared (8–14 μm) regions. As a result, they are unable to detect gases with absorption peaks in both spectral bands simultaneously (Dong et al., 2017). For instance, gases such as carbon dioxide (CO2) has an absorption peak at 4.4 μm in the mid-infrared band, and sulfur hexafluoride (SF6) has an absorption peak at 10.6 μm in the long-infrared band, these two gases cannot be simultaneously detected by conventional cameras due to their restricted spectral coverage. To overcome this limitation, this paper propose a broadband infrared imaging system optimized for the 3–14 μm wavelength range, which can detect gases across both the mid- and long-infrared bands, thereby demonstrating the significant advantage of broadband infrared imaging for comprehensive gas leak detection.

2 IMAGING SYSTEM DESIGN

To achieve broadband infrared gas imaging, a passive imaging system based on a broadband infrared camera is designed. The system's design is primarily informed by the layer radiative transfer model of passive infrared imaging and the absorption characteristics of the target gas in the infrared spectrum.

The layer radiative transfer model is commonly employed in passive infrared gas imaging (Flanigan, 1996). It conceptualizes radiative transfer as a series of parallel transmission layers, where each layer receives input radiation from the preceding layer and emits output radiation to the subsequent layer. Assuming a uniform atmospheric distribution between the background and the infrared camera, the multilayer radiative transfer model can be simplified into a three-layer system, as depicted in Figure 1. Here, I_g represents the radiation intensity of the gas cloud, and I_t indicates the intensity of background radiation after absorption by the gas cloud. In upper path, when the gas cloud is present, the equivalent temperature detected by the infrared camera is expressed by $T(I_t + I_g)$. The Noise-Equivalent Temperature Difference (NETD) of the infrared detector should also be considered. According to the detection principles of the infrared camera, when the temperature difference between the target and the background within the radiation system is less than the NETD, the gas cloud in the foreground cannot be accurately distinguished from the background. This condition is described by the following equation (Olbrycht and Kałuża, 2019).

$$|T(I_B) - T(I_t + I_g)| > NETD$$

The background radiation after being absorbed by the gas cloud is expressed using the basic Lambert-Beer law of spectral absorption (Claps et al., 2001):

$$I_T = I_B * e^{-\alpha(\lambda)LC}$$

Where $\alpha(\lambda)$ is the absorption cross-section of the gas at wavelength λ, L is the length of the gas absorption path, C is the concentration of the target gas.

Therefore, NETD of the infrared camera is a critical factor in imaging system design. It directly determines the gas detection system's performance. Additionally, increased gas concentrations and extended absorption paths result in greater contrast in the background radiation after passing through the gas cloud, thereby making the gas trace more detectable.

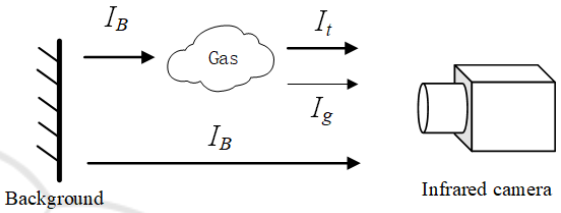

Figure 1: Principle of passive infrared gas imaging.

The absorption characteristic spectra of gas molecules are typically concentrated in the mid- to long-wave infrared regions, specifically in the 3-14 μm range (Meribout, 2021). By imaging a specific gas within its corresponding spectral band, the gas can be detected.

Sulfur hexafluoride (SF_6) and carbon dioxide (CO_2) are two gases widely utilized in industrial production and common infrastructure applications (Zhou et al., 2018) (Yu et al., 2012). Their absorption characteristic spectra are available from the HITRAN database (Gordon et al., 2022). The absorption peaks of CO_2 and SF_6 located around 4.4 μm and 10.6 μm, as shown in Figure 2 and 3 respectively, where x axis is the wavelength in μm, y axis is the corresponding spectral line intensity, represented by wavenumbers per column density.

Based on the aforementioned principle of infrared broadband gas imaging detection, we have developed an infrared broadband imaging system for gas leak detection and gas composition analysis. The system primarily comprises a broadband lens and an uncooled infrared focal plane camera(IRAY RTD611WB). The schematic diagram of the system is depicted in Figure 4.

The broadband infrared lens is specifically designed and optimized for the 3-14 μm wavelength. Due to the broadband operating wavelength, two infrared materials germanium (Ge) and zinc selenide

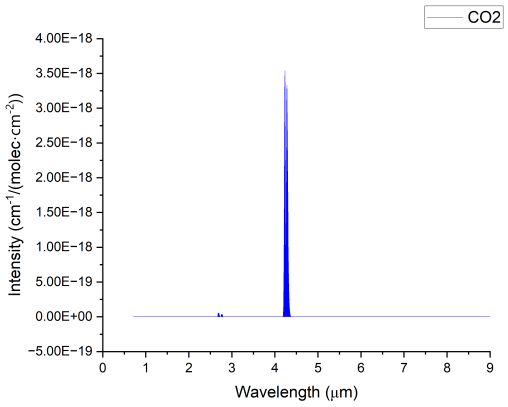

Figure 2: Infrared absorption spectrum of CO_2.

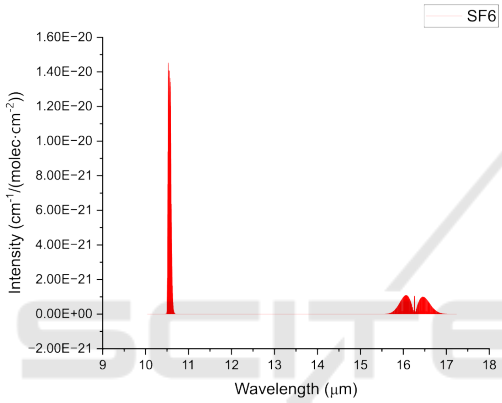

Figure 3: Infrared absorption spectrum of SF_6.

(ZnSe) are utilized to minimize potential chromatic aberration. Additionally, four aspherical surfaces are integrated to further optimize aberrations, as shown in Figure 5. The lens has a focal length of 50 mm and an aperture of 40 mm, resulting in an F-number of 1.25. Combined with the focal plane camera's target surface of 10.8 × 8.8 mm, the optical system achieves a field of view (FOV) of 12.8° × 10°. The average transmittance of the lens across the entire 3-14 μm range is not less than 80%. Given the detector's pixel size of 17 μm, the lens resolution must be at least 29.4 lp/mm. According to the modulation transfer function (MTF) diagram, the lens contrast ratio at 30 lp/mm is not less than 0.4, thereby satisfying the design specifications.

3 ALGORITHM DESIGN

Once the gas image is captured through the imaging system, image processing algorithms should be applied to segment the region where the gas is present. For gas leak detection algorithms, both

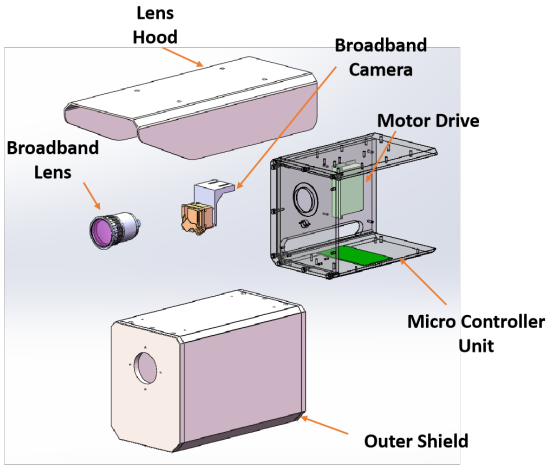

Figure 4: System diagram.

traditional image processing methods, such as the image difference algorithm based on OpenCV, and gas target detection algorithms utilizing deep learning techniques, have been explored. In this study, both types of algorithms are evaluated, leading to the development of a novel adaptive gas leakage detection algorithm that integrates elements from the aforementioned methods.

A. Gas Detection Algorithm Based on YOLOX

To identify gas leakage in infrared images, this study employs a gas target detection model based on YOLOX. This is a deep learning model belongs to the YOLO(You Only Look Once) algorithm series (Ge et al., 2021). It has the feature of enhanced detection efficiency, which is suitable for the dynamic scenarios of gas detection. Initially, the infrared image size is adjusted, and downsampling is performed to compress the image, thereby reducing the computational load during the detection process. Subsequently, the YOLOX gas leak detection model is applied to adjust the image channels and extract relevant features. These features are then input into a feature pyramid for fusion, enhancing the overall feature extraction process. Based on the extracted features, the model predicts the presence of a gas leakage target in the infrared image, generating a detection result. This result not only indicates whether a gas leakage is present but also identifies the specific region of the leak within the image.

It is important to note that the gas leak detection model is a pre-trained deep learning network capable of identifying gas leaks in infrared images. In this study, the YOLOX deep learning network is selected. Compared to traditional target recognition algorithms, YOLOX demonstrates higher accuracy in generalization scenarios. YOLOX also have superior

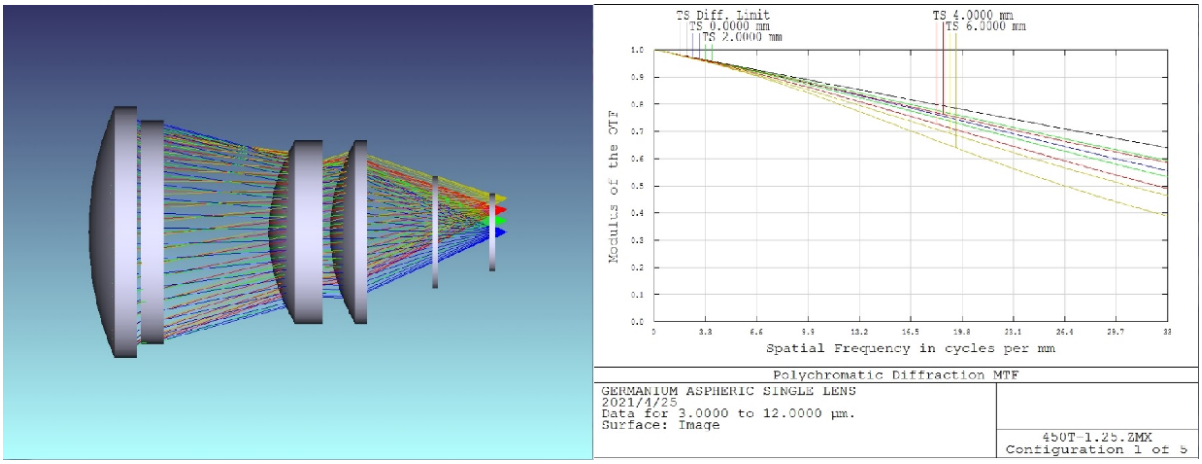

Figure 5: Lens design diagram.

real-time performance compared to models with large number of parameters like Vision Transformer. This is appropriate for deployment in resource-constrained environments, demonstrating effective performance even with limited training data.

B. Background Difference Algorithm Based on OpenCV

For gas trace extraction, this study proposes a gas leak detection algorithm utilizing traditional OpenCV image processing techniques, specifically designed for detecting gas leak traces in the 3–14 µm band infrared images. The implementation steps are as follows:

1) Background Differentiation: A differential image is obtained by subtracting the background image (without gas leakage) from the target image (with gas leakage). The resulted differnetial image has the same pixel dimensions with the original image. To minimize the impact of noise, multiple differential images are averaged, which is similar to smoothing in time domain. The differential image is then normalized, expressed as follows:

$$I(x,y) = \begin{cases} 0 \\ \frac{I_{max}}{I(x,y)} \times 255 \end{cases}$$

2) Image Filtering: The normalized differential images are processed using median filtering and bilateral filtering to obtain filtered images. A threshold is then applied, where pixel values exceeding the threshold are retained, and those below are set to zero, thus isolating the gas traces within the images.

3) Image Merge: The filtered image is added with the target image containing the gas leakage, resulting in the final merged image.

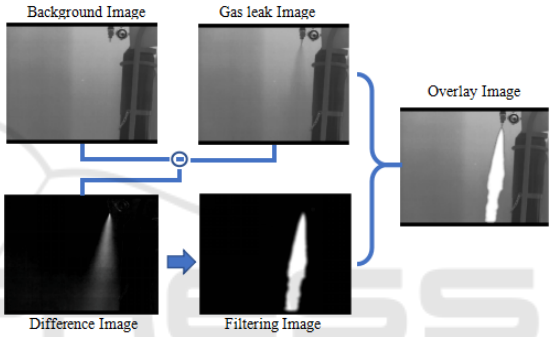

Figure 6: Gas segmentation based on differential and filtering.

C. Adaptive Gas Leakage Comprehensive Detection Algorithm

The process for the adaptive gas leakage comprehensive detection algorithm proposed in this manuscript is depicted in Figure 7. Initially, a detection threshold of the gas leak detection model is set. The infrared images captured by the imaging system are input into the YOLOX model for preliminary detection. If no gas leakage is detected, the detection threshold is lowered, and the newly acquired infrared images are subsequently screened until the minimum threshold value is reached, or a gas leakage target is detected in any infrared image. If gas leakage is detected, the image area containing the gas target is identified by the location of the regression box. Based on the detection results from each infrared image, images with detected gas leaks are classified as gas leak images, whereas those without detected leaks are considered background images. This enables the automatic selection and updating of the background, facilitating future regional background differentiation based on the classified gas leak and background images.

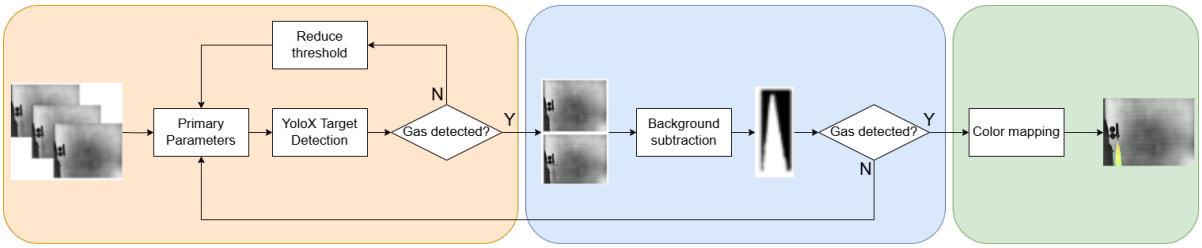

Figure 7: Diagram of adaptive detection algorithm.

After gas leak is detected as previously described, a background difference algorithm is employed for detailed examination of the infrared image region containing the detected leak. This step aims to validate the presence of a gas leak within the regression box and eliminate any false detection from preliminary results. If a false detection is identified, the initial threshold for the gas leak detection model is restored, and the target detection process recommences. Conversely, if a gas leak is confirmed, the region of the infrared image containing the leak is enhanced for display and output.

To further exhibit the gas distribution within the specific leakage area, jet color mapping is used to represent the concentration of leaked gases. Jet color mapping is a visualization technique that assigns colors to data values based on a predefined color gradient. Typically, the jet color map ranges from red to green to blue, providing a spectrum that represents varying data intensities, corresponding color scheme is shown in Figure 8. In the context of gas leak detection, this mapping method is used to represent the density of gas in a visually intuitive manner. High-density regions are colored red, indicating a critical concentration of gas, while lower-density areas transition through yellow and ultimately to green, signifying lower gas concentrations.

By mapping gas density to colors, jet color mapping allows for an easy and immediate understanding of gas distribution patterns. This approach is particularly useful in applications such as gas leak detection, where rapid evaluation is essential. The color-coded representation enables personnel to identify high-risk areas effectively, facilitating timely responses to potential hazards.

Figure 8: Color scheme of jet color mapping.

In these application scenarios, continuous detection of gas leaks is achieved. Through preliminary and detailed detection, the likelihood of false detection is minimized while ensuring real-time capabilities. Furthermore, adaptive adjustment to the detection threshold reduces dependency on background conditions, effectively enhancing the accuracy of gas leak detection.

4 EXPERIMENT AND RESULT ANALYSIS

The proposed broadband infrared imaging system was evaluated through controlled field experiments to assess its capability in detecting and characterizing gas leaks. Three scenarios were analyzed involving the release of SF_6 and CO_2, and a combination of both gases. The flow rate for each release was controlled to approximately 25 L/min using a valve, and the resulting plumes were visualized using jet color mapping to exhibit concentration gradients. The segmented results are shown in Figure 9a, 9b and 9c.

In the first experiment, SF_6 was released from a gas cylinder, and the broadband imaging system effectively recorded and segmented the gas plume (Figure 9a). The concentration gradient was represented with colors ranging from red (highest concentration) to blue (lowest concentration), demonstrating the ability of the system to effectively capture and visualize the gas distribution.

In the second experiment, CO_2 was released under the same conditions (Figure 9b). While the concentration gradient was visualized similarly, the segmented area of CO_2 appeared smaller compared to SF_6. This was attributed to the broadband infrared camera's relatively better response in the long-infrared range (8–14 µm), where SF_6 has a significant absorption peak at 10.6 µm. Despite the difference in sensitivity, the system effectively detected and visualized the CO_2 plume.

The third experiment involved the simultaneous release of SF_6 and CO_2 from separate sources (Figure 9c). The broadband imaging system captured and distinguished both gases in real time, illustrating their respective concentration gradients using jet color mapping. The ability to segment and visualize both gases within a single scene demonstrates

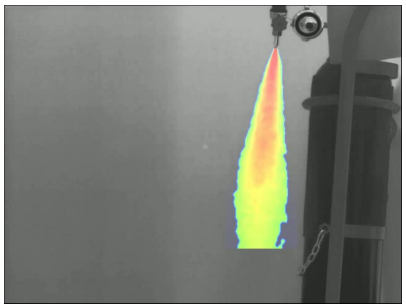

(a) Segmentation results of SF_6.

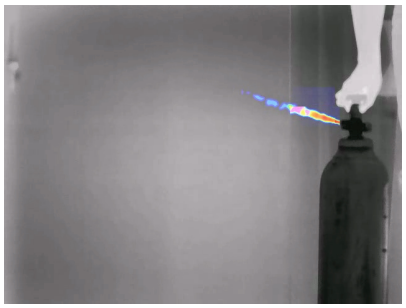

(b) Segmentation results of CO_2.

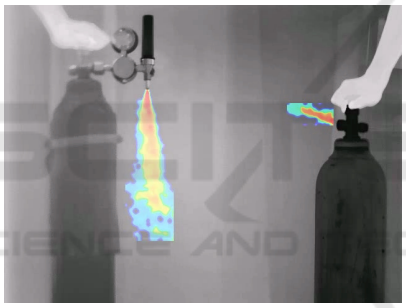

(c) Segmentation results both CO_2 and SF_6.

Figure 9: Segmentation results of three images.

the system's unique capability for simultaneous detection and differentiation of multiple gases. Conventional infrared cameras, which are typically limited to either the mid-infrared (3–5 µm) or the long-infrared (8–14 µm) range, would be unable to simultaneously detect gases that absorb in different spectral bands. The broadband system, by covering the full 3–14 µm range, effectively demonstrated its versatility and superiority in simultaneously capturing and analyzing multiple gases with distinct spectral characteristics. This capability is particularly beneficial in real-world industrial scenarios where multiple gases may be present.

Overall, the results demonstrated the broadband infrared imaging system's robust capability to detect and visualize different gases simultaneously. The broadband capability, covering both the mid- and long-infrared spectral ranges, enabled comprehensive gas detection that conventional infrared cameras could not achieve. This makes the system particularly suitable for industrial applications requiring accurate and simultaneous detection of multiple gases.

5 CONCLUSION

This paper presents a broadband passive infrared imaging system for the detection of gas leaks. The system, incorporating a wide-spectrum lens and an uncooled infrared focal plane array, has been optimized for operation across the 3–14 µm wavelength range, providing flexibility in detecting a wide variety of gases. The proposed hybrid gas detection algorithm integrates both deep learning-based (YOLOX) and traditional image processing methods, thereby enhancing the system's sensitivity and reliability in analyzing gas leaks under realistic field conditions. Experimental validation using CO2 and SF_6 gases, with distinct absorption peaks in the mid- and long-infrared regions, demonstrates the efficacy of the system for broadband gas detection.

Unlike conventional infrared cameras, which are limited to either the mid- or long-infrared range, the proposed broadband system offers the capability to detect gases with absorption peaks in both spectral bands simultaneously. This unique capability is crucial for comprehensive gas detection in diverse industrial and environmental applications. Future research will focus on the further optimization of the optical system to enhance sensitivity and the development of advanced machine learning models for gas detection applications.

REFERENCES

Claps, R., Englich, F. V., Leleux, D. P., Richter, D., Tittel, F. K., and Curl, R. F. (2001). Ammonia detection by use of near-infrared diode-laser-based overtone spectroscopy. *Applied Optics*, 40(24):4387–4394.

Dong, M., Zheng, C., Miao, S., Zhang, Y., Du, Q., Wang, Y., and Tittel, F. K. (2017). Development and measurements of a mid-infrared multi-gas sensor system for co, co2 and ch4 detection. *Sensors*, 17(10):2221.

Flanigan, D. F. (1996). Limits of passive remote detection of hazardous vapors by computer simulation. In *Electro-Optical Technology for Remote Chemical Detection and Identification*, volume 2763, pages 117–127. SPIE.

Ge, Z., Liu, S., Wang, F., Li, Z., and Sun, J. (2021). Yolox: Exceeding yolo series in 2021.

Gordon, I. E., Rothman, L. S., Hargreaves, e. R., Hashemi,

R., Karlovets, E. V., Skinner, F., Conway, E. K., Hill, C., Kochanov, R. V., Tan, Y., et al. (2022). The hitran2020 molecular spectroscopic database. *Journal of quantitative spectroscopy and radiative transfer*, 277:107949.

Kulp, T. J., Powers, P. E., and Kennedy, R. B. (1997). Remote imaging of controlled gas releases using active and passive infrared imaging systems. In *Infrared technology and applications XXIII*, volume 3061, pages 269–278. SPIE.

Meribout, M. (2021). Gas leak-detection and measurement systems: Prospects and future trends. *IEEE Transactions on Instrumentation and Measurement*, 70:1–13.

Moshayedi, A. J., Sohail Khan, A., Hu, J., Nawaz, A., and Zhu, J. (2023). E-nose-driven advancements in ammonia gas detection: a comprehensive review from traditional to cutting-edge systems in indoor to outdoor agriculture. *Sustainability*, 15(15):11601.

Nutt, K. J., Hempler, N., Maker, G. T., Malcolm, G. P., Padgett, M. J., and Gibson, G. M. (2020). Developing a portable gas imaging camera using highly tunable active-illumination and computer vision. *Optics Express*, 28(13):18566–18576.

Olbrycht, R. and Kałuża, M. (2019). Optical gas imaging with uncooled thermal imaging camera-impact of warm filters and elevated background temperature. *IEEE Transactions on Industrial Electronics*, 67(11):9824–9832.

Strahl, T., Herbst, J., Lambrecht, A., Maier, E., Steinebrunner, J., and Wöllenstein, J. (2021). Methane leak detection by tunable laser spectroscopy and mid-infrared imaging. *Applied Optics*, 60(15):C68–C75.

Tan, L., Feng, Z., Zheng, H., Yao, Z., Weng, X., Wang, F., and Chang, Z. (2022). Development trend of electronic nose technology in closed cabins gas detection: a review. *Applied Sciences*, 12(18):9326.

Wurst, N. P., Meola, J., and Fiorino, S. T. (2017). Improved atmospheric characterization for hyperspectral exploitation. In *Algorithms and Technologies for Multispectral, Hyperspectral, and Ultraspectral Imagery XXIII*, volume 10198, pages 116–122. SPIE.

Yu, C.-H., Huang, C.-H., Tan, C.-S., et al. (2012). A review of co2 capture by absorption and adsorption. *Aerosol and air quality research*, 12(5):745–769.

Zhao, N., Zhao, D., Ma, L., and Wang, B. (2022). Study on a photoacoustic spectroscopy trichloromethane gas detection method based on an arched photoacoustic cavity. *Analytical Methods*, 14(15):1507–1514.

Zhou, A., Gao, L., Ji, X., and Zhang, M. (2018). Research and application of sf6/n2 mixed gas used in gis bus. *Power Syst. Technol*, 42(10):3429–3435.